Heliyon 8 (2022) e10609

Contents lists available at ScienceDirect

Heliyon

journal homepage: www.cell.com/heliyon

Research article

Structural, nonlinear optical and antimicrobial properties of sol-gel derived, Fe-doped CuO thin films

Mohammad Humaun Kabir [a], Humayra Ibrahim [a], Sikder Ashikuzzaman Ayon [a], Md. Muktadir Billah [a,*], Sharif Neaz [b]

[a] Department of Materials and Metallurgical Engineering, Bangladesh University of Engineering and Technology, Dhaka, Bangladesh
[b] Department of Chemistry, Dhaka Commerce College, Dhaka, Bangladesh

ARTICLE INFO

Keywords:
Thin film
Sol-gel
Band gap
Optical conductivity
Antimicrobial

ABSTRACT

Undoped and Fe-doped CuO thin films with different weight ratios (3, 6, and 9 wt.% of Fe) were deposited onto glass substrates using the sol-gel spin coating technique. X-ray diffraction analysis of these samples indicated that all the films were polycrystalline, and crystallite size decreased with doping concentration. As revealed by scanning electron microscopy, Fe doping increased average particle size and improved size distribution in films. The bandgap of undoped CuO thin film was tuned from 3.48 to 2.79 by the addition of 9 wt.% Fe, and reasonable explanations have been presented. Optical parameters, such as refractive index, extinction coefficient, dielectric constant, and optical conductivity, were calculated for optoelectronic applications. Finally, antimicrobial properties were measured for their possibility to be used as disinfectants, and the antifungal activity of Fe-doped CuO thin films was shown to be more effective.

1. Introduction

Many semiconductor materials are in sophisticated use or being evaluated for use in different fields, including the photovoltaic industry, microelectronics, biotechnology, etc., due to their unique properties, typically resulting from quantum size effect, and high surface area. Recently, copper oxide-based nanostructure has been recognized as a promising candidate for technical revolution owing to its extensive use in many significant fields of photovoltaic cells [1], antibacterial activities [2], gas sensing [3], ultraviolet sensing [4], magnetic storage media [5], supercapacitors [6], etc., which can be attributed to its excellent electrical and optical properties [7]. In this regard, CuO is an important p-type semiconductor with a narrow and direct optical bandgap of 1.5 eV at room temperature [8]. Experimental studies reported that the excess of oxygen or copper vacancies is responsible for this p-type conductivity in CuO [9].

A range of forming processes is available to prepare nanostructured CuO thin films, such as chemical vapor deposition [10], magnetron sputtering [11], electrodeposition technique [12], reflux condensation [13], SILAR method [14], sol-gel spin-coating process [15], pulsed laser technique [16], ex-situ and solvent casting technique [17] and so on. When compared to most thin-film synthesis methods, the sol-gel spin-coating process has significant advantages such as molecular composition mixing, low processing temperature, and economic viability [18, 19]. Immense research has been done to improve CuO thin films by optimizing different process parameters [20].

To enhance the physical and chemical properties of materials for specific applications, dopants can be incorporated into them. Since copper has three oxidation states [21], i.e., Cu^{+}, Cu^{2+}, and Cu^{3+}, both hole doping, and electron doping mechanisms are possible. By bringing radical changes in the optical, electrical, and magnetic properties of CuO, transition metal doping has recently gained a lot of attention and found outstanding utility in solid-state electronics [22, 23, 24, 25, 26]. Ni-doped CuO thin films show higher absorption, charge carrier density, and photostability than pure CuO films [20, 23, 27, 28]. Fe^{2+} doping increases Cu^{2+} formations and oxygen vacancy in CuO thin films, which increases bandgap slightly while significantly improving conductivity and mobility [29]. Click or tap here to enter text. Doping with Cd [30], La [31], or Ba [32] has significant impacts on CuO thin films as they improve photosensitivity, which is useful for photocatalysis, hydrogen production, and photodetection applications. Tuning bandgap and enhancement of 4-nitrophenol degradation can be achieved by Ag doping [33]. Co^{2+} and Fe^{3+} co-doping shows complete degradation efficiency in photocatalysis after 12 h of exposure to sunlight [34]. Due to significant

* Corresponding author.
E-mail address: mbillah@mme.buet.ac.bd (Md.M. Billah).

https://doi.org/10.1016/j.heliyon.2022.e10609
Received 7 March 2022; Received in revised form 20 April 2022; Accepted 7 September 2022

capacitance value and potential window, highly doped Ru-based CuO can be considered for superconducting materials [35]. Moreover, extensive research on CuO nanoparticles and nanostructured thin films has been conducted for obtaining room-temperature ferromagnetism [36, 37, 38, 39]. Reducing particle size [38] and forming complex compounds with magnetic ions can introduce magnetic properties in non-magnetic and antiferromagnetic materials, introducing super-exchange interaction due to the magnetic relaxation of ions in the materials [40]. Highly doped CuO thin films with Mn^{2+} (15–30 wt.%) shows magnetic properties at low temperature because of ferromagnetic coupling between Mn and Cu ions [37, 41, 42]. 10 w.% Fe^{2+} doping shows significant coercivity in CuO thin films at room temperature [39]. Finally, CuO thin film shows noteworthy activity against both bacteria and fungi. Pure CuO films can be considered antibacterial agents due to having more than 20 mm inhabitation zone against S. aureus and 11–15 mm for E. coli [43]. Doping with Vanadium can enhance these antimicrobial properties, particularly against *E. Coli*, *K. Pneumonia*, *S. Aureus*, and *P. Aeruginosa* [44].

Previously, Fe-doped CuO thin films have been investigated for optical, electrical, and magnetic properties, and synthesized by various methods [39, 45, 46]. However, very few papers are reported on Fe-doping CuO thin films by following the spin-coating sol-gel method [29, 34], and research outcomes are still far away from expectations. In this paper, the structural, morphological, and optical properties have been investigated to understand the relation between crystalline phases and grain size with absorption and bandgap of the Fe-doped thin films. Besides, UV-visible spectra are thoroughly examined for comprehending optical constants, such as refractive index, extinction coefficient, dielectric constants, and optical conductivity. Finally, to the best of our knowledge, for the first time antibacterial and antifungal investigation is presented in this publication for Fe-doped CuO thin films prepared by sol-gel spin coating.

2. Experimental details

2.1. Thin film synthesis

The nanocrystalline pure CuO and Fe-doped CuO thin films were prepared by the sol-gel spin-coating technique. 0.2 M copper acetate monohydrate [$Cu(COOCH_3)_2H_2O$] was dissolved in the solvent of 2-methoxyethanol [$CH_3OCH_2CH_2CH_2OH$]. 3, 6, and 9 wt.% iron was doped, and ferric nitrate nonahydrate [$Fe(NO_3)_3.9H_2O$] was used as the source of dopant. After constant magnetic stirring for 10 min at room temperature, monoethanolamine [$OHCH_2CH_2NH_2$] was added as a stabilizer maintaining a 1:1 mole ratio with precursor. Later, the solution was stirred for 1 h at 70 °C and aged for 24 h at room temperature.

Before film deposition, the soda-lime-silica glass substrates were successively cleaned with acetone, ethanol, and deionized water. A two-step spinning system was followed to obtain the uniform films. First, the solution was spread onto the substrate at 100 rpm for 15 s, and then for further spreading the next cycle at 3000 rpm for 20 s. The deposition process was repeated four times, and each time deposited film was dried immediately on the hotplate for 10 min at 160 °C. All thin films were annealed for 1 h at 500 °C in air conditioning.

2.2. Structural and optical characterization

X-ray diffraction (Empyrean PANalytical) was used to determine the crystal structure of the annealed CuO films using Cu K_α radiation. Crystallite size, lattice parameters, strain, and dislocation density of the films were obtained by Rietveld refinement using HighScore Plus software. Structural morphology along with film thickness was studied by field emission scanning electron microscope (FE SEM: JEOL, JSM, 7600F). An ultraviolet-visible scanning spectrophotometer (Halo DB-20/DB-20S UV-vis) recorded the absorbance and transmittance spectra.

2.3. Antimicrobial test

Kirby-Bauer antibiotic testing method was used to carry out antimicrobial studies [47]. Known quantities of bacteria are grown on agar plates in the presence of thin wafers containing relevant antibiotics. *Bacillus cereus*, *Staphylococcus aureus*, and *Streptococcus mutans* were used as gram-positive bacteria, whereas *Escherichia coli* and *Pseudomonas aruginosa* were used as gram-negative bacteria. The density of each microbial suspension was adjusted to be equal to that of 108 CFU/ml (standardized by 0.5 McFarland standards) and used as the inoculum for performing the agar well diffusion assay. The suspension was then diluted at 1:100 in Mueller-Hinton broth to get 106 CFU/ml. Standard ciprofloxacin (10.0 μg/disc) and Clotrimazole discs were used as positive controls to ensure the activity of standard antibiotics against the test organisms as well as to compare the response produced by the known antimicrobial agent with that produced by the test sample. Blank discs were used as negative controls to ensure that the residual solvents (leftover discs even after air-drying) and the filter paper were not active themselves. For fungus, inocula were prepared according to Shehata et al. [48], by counting conidia harvested from ~7-day-old potato dextrose agar cultures in a hemocytometer, followed by adjustment to the appropriate final density. Results were read after 48 h incubations for Candida albicans species. Clotrimazole was used as a positive control, and discs soaked with chloroform and then dried were used as a negative control. The zone of incubation (ZOI) was analyzed after incubation.

3. Results and discussion

3.1. Structural properties

Figure 1 shows the XRD patterns of annealed pure and Fe-doped CuO thin films deposited on silica glass substrates. The spectra were recorded in the 2θ range of 25°–70°, which is well-matched with standard ICDD data code 01-080-076. These films present two strong peaks at 35.53° and 38.64°, corresponding to ($\bar{1}11$) and (111) planes of the pure CuO phase, respectively. In addition, other characterization peaks are identified at 48.85°, 53.35°, 58.16°, 61.51°, 66.34°, and 68.02°, corresponding to ($\bar{2}02$), (020), (202), ($\bar{1}13$), (022), and (220) planes, respectively. Identification of these characterization peaks of pure monoclinic CuO, along with the absence of any additional peaks, show that all the films are polycrystalline, having a monoclinic crystal

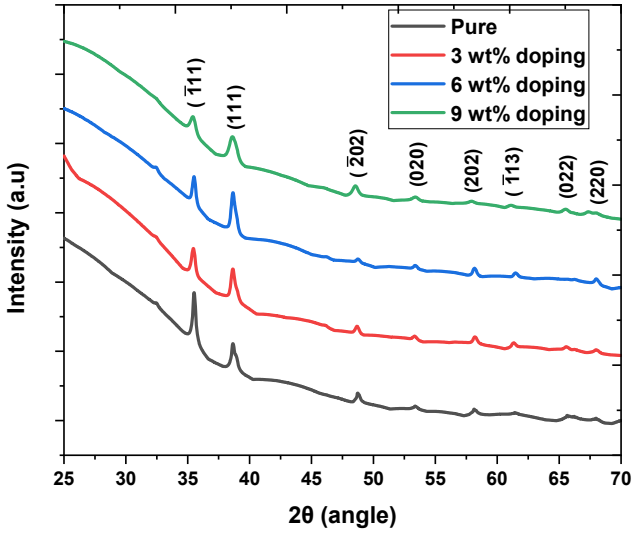

Figure 1. X-ray diffraction of pure along with 3, 6 and 9 wt.% Fe-doped CuO thin films.

structure [49]. The intensity of ($\bar{1}11$) plane was suppressed drastically with increasing doping concentration; However, the intensity of the (111) plane increased up to 6 wt.% doping. The increasing relative intensity of (111) plane compared to ($\bar{1}11$) plane in Table 1 reveals the preferential growth of CuO along the (111) plane with increasing doping concentration. Furthermore, decreasing both peak intensities at 9 wt.% doping concentration indicates a continuous increase in lattice imperfections [20]. As the percentage of ionic radius difference between Cu^{2+} (0.73 Å) and Fe^{3+} (0.64 Å) is 12.32%, Cu^{2+} ions can be replaced by a certain percentage of Fe^{3+} ions doping without disturbing the crystal structure. Therefore, no extra peaks were found for any impurity phases like α-F_2O_3, β-F_2O_3, F_3O_4, and $CuFe_2O_4$ [50].

Crystallite size, dislocation density, and strain were calculated for the peak of the (111) plane, where the peak shape is fitted with Gaussian mode. Debye-Scherrer's equation used for calculating crystallite size is given as follows in Eq. (1):

$$\text{Crystallite size}, D = \frac{k\lambda}{\beta \cos\theta} \quad (1)$$

here, K is the shape factor which equals 0.94, λ is the wavelength of the incident X-ray beam (1.5418 Å), θ is half of the Bragg diffraction angle, and β in radian is the peak width at half maximum (FWHM). Crystallite size was decreased with increasing doping concentration since increasing doping concentration caused increasing crystal distortions and thus retard the growth of the individual crystals. Similar studies have been reported for Fe-doped CuO thin films [34], Fe-doped CuO nanoparticles [50], and Fe-doped ZnO nanoparticles [51] earlier. Dislocation density (∂) and strain (ε) are calculated from the following Eqs. (2) and (3) [20]:

$$\partial = \frac{1}{D^2} \quad (2)$$

$$\varepsilon = \frac{\beta \cos\theta}{4} \quad (3)$$

Table 1 shows that dislocation density and strain increase with increasing doping concentration. The positions of the peak do not change with increasing doping percentage. Lattice parameters and cell volume of undoped and Fe-doped CuO thin films remained almost similar except for 9 wt.% doping concentrations. Thus, doping with Fe has no major influence on crystal structure because of the combination of atomic substitution and cation vacancy in the pure CuO structure [52].

3.2. Morphological observations

SEM micrographs of pure CuO thin films' cross-sections are shown in Figure 2(a, b), where the thickness of these films is estimated to average 116 nm. The grain size of pure CuO thin films is an average of 43.63 nm with a standard error of 1.25, presented in Figure 2(c, d). 3 wt.% Fe doped CuO thin films in Figure 2(e, f) showed the most uniform (lowest standard error) grain structure having an average grain size of 52.68 nm. Furthermore, average grain size and standard error increase more for 6 wt.% and 9 wt.% doping, as shown in Figure 2(g, h, i, j). These grain growths can result from accelerated diffusion, a small radius of Fe^{3+} ions, and lower activation energies with increasing doping concentration [53, 54].

3.3. Optical properties

The absorbances of pure and Fe-doped CuO thin films are measured for analyzing nonlinear optical properties by UV-Vis scanning spectrophotometer, presented in Figure 3(a). Absorbance decreases continuously with increasing doping concentration as the doping element reduces the structural and morphological properties of the films [55]. Reducing crystallite size with increasing doping concentration, as shown in Table 1, can result in the decreasing light absorption of the films [56].

Furthermore, the transmittance of these films, illustrated in Figure 3(b), was calculated from absorbance data using the following Eq. (4):

$$A = 2 - \log 10\,(\%T) \quad (4)$$

Average transmittance in the visible range (430–770 nm) is raised from 34% to 43% with increasing doping concentration, as shown in Table 2. Optical absorption data are used to calculate the absorption coefficient and bandgap. Here, the absorption coefficient was determined using Eq. (5),

$$\alpha = \frac{1}{t} \ln\left(\frac{A}{T}\right) \quad (5)$$

where α is the absorption coefficient in cm^{-1}, and t is the thickness of the films. The direct optical band gap of these films was calculated by using the Tauc formula, shown in Eq. (6):

$$(\alpha h\upsilon)^2 = A\,(h\upsilon - Eg) \quad (6)$$

Table 1. XRD data of the films.

Dopant Concentration (wt.%)	Crystallite Size (nm)	Intensity Ratio of (111) to ($\bar{1}$ 11)	Dislocation Density (m^{-2})	Strain	Lattice Parameters (Å)	c/a Ratio	Cell Volume (Å^3)
0	20.02	0.53	2.495×10^{15}	0.099	a = 4.682199	1.101	81.68
					b = 3.432803		
					c = 5.152446		
					β = 99.48188		
3	19.60	1.19	2.603×10^{15}	0.101	a = 4.686809	1.097	81.57
					b = 3.430347		
					c = 5.142134		
					β = 99.36250		
6	18.47	1.33	2.931×10^{15}	0.108	a = 4.685600	1.098	81.47
					b = 3.429282		
					c = 5.139109		
					β = 99.35455		
9	15.41	1.23	4.216×10^{15}	0.129	a = 4.689392	1.104	82.10
					b = 3.428238		
					c = 5.176154		
					β = 99.39385		

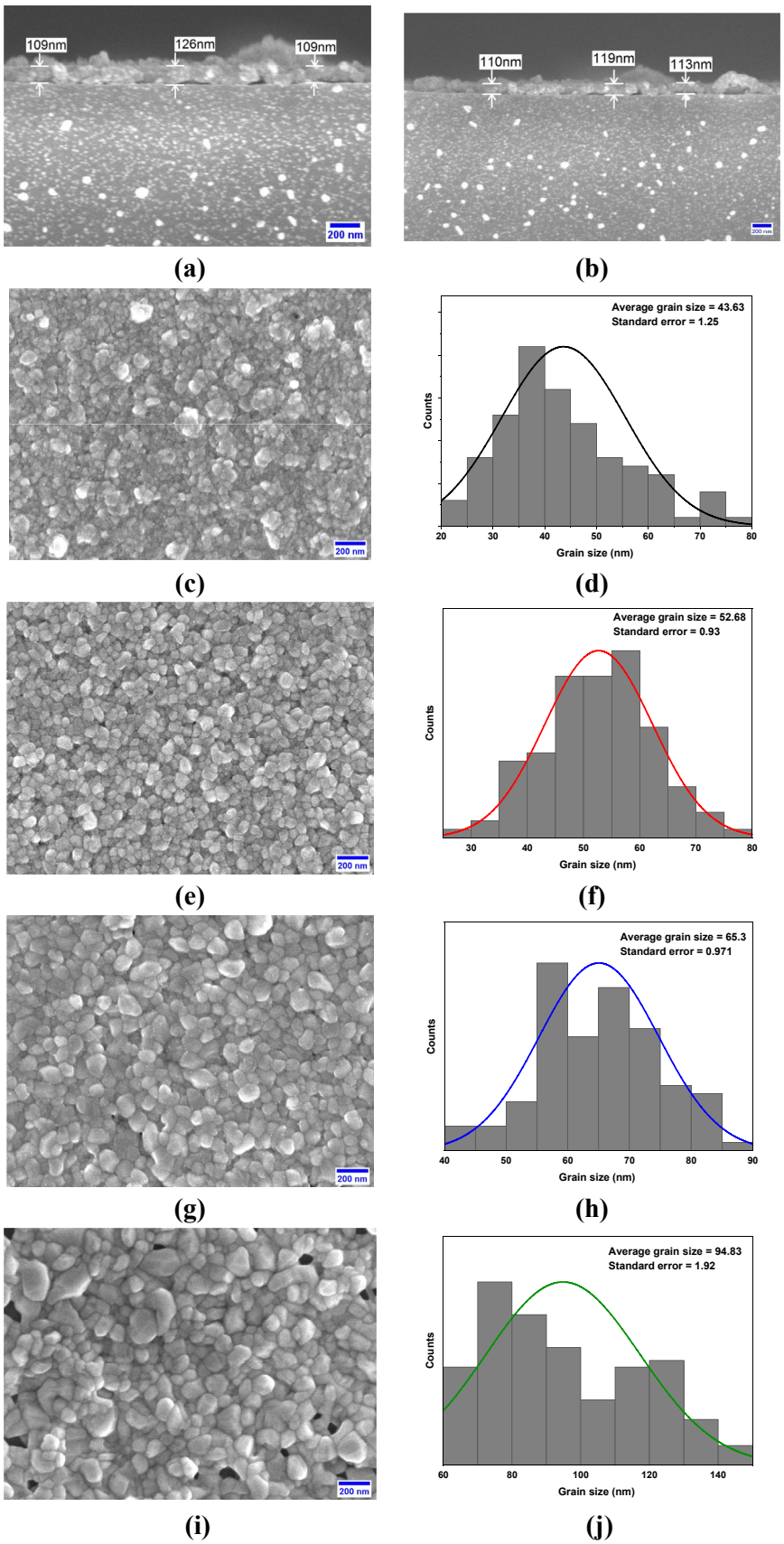

Figure 2. SEM images of (a–b) Cross-section of CuO thin films, morphology and size distribution of (c–d) pure, (e–f) 3 wt.%, (g–h) 6 wt.% and (i–j) 9 wt.% Fe-doped CuO thin film.

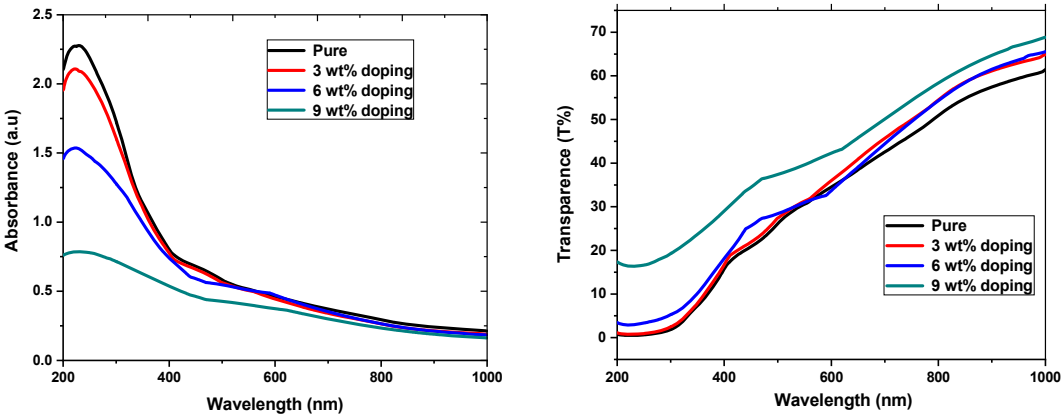

Figure 3. UV-vis spectra of pure and Fe-doped CuO thin films (a) absorbance, (b) transmittance.

Table 2. Optical properties of pure and Fe-doped CuO thin films.

Dopant Concentration (wt.%)	Average Transmittance in Visible Range	Band Gap (eV)	Absorption Edge (nm)
0	34	3.48	356
3	35	3.44	360
6	37	3.18	390
9	43	2.79	444

Here, h is the Plank's constant, υ is the frequency of the incident photon, A is a constant called the band tailing parameter, and E_g is the optical direct band gap energy. From the plot in Figure 4, pure CuO shows a 3.48 eV bandgap, which is relatively higher than bulk CuO nanoparticles. This can be attributed to the factors like oxygen stoichiometry, quantum confinement size effect, and microcrystals with different morphologies [57, 58].

With increasing doping concentration, the bandgap decreased from 3.48 eV to 2.79 eV, as presented in Table 2. Accordingly, Absorbance edges shift to a longer wavelength (red-shift) from 356 nm to 444 nm with increasing doping concentration, also shown in Table 2. The shift of bandgap and absorption edge can be attributed to the tail-like effect with the heavily doping element where large numbers of impurities are inserted in the host lattice. Each impurity ion locally introduces a distinct energy level, and these levels interact to form a band [59].

The value of the refractive index (n) and extinction coefficient (k) were determined using the following Eqs. (7) and (8) respectively,

$$n = \frac{1}{T} + \sqrt{\frac{1}{T-1}} \tag{7}$$

$$k = \frac{\alpha\lambda}{4\pi} \tag{8}$$

here, T is the transmittance and α is the absorbance coefficient. Variations of refractive index and extinction coefficient with respect to wavelength are presented in Figure 5. The refraction index is found to decrease with increasing doping concentration which can be attributed to the retarded crystal growth due to increasing doping concentration [60]. The extinction coefficient of these films is comparatively low, which indicates the smoothness of the surface and homogeneity of the particle size. The decrease of extinction coefficient with increasing doping concentration represents lower absorption in higher doping [61].

The value of real and imaginary parts of the dielectric constant was measured using the following Eqs. (9) and (10), accordingly,

$$\varepsilon_r = n^2 - k^2 \tag{9}$$

$$\varepsilon_i = 2nk \tag{10}$$

here, ε_r and ε_i are real and imaginary parts of the dielectric constant, respectively, which are presented in Figure 6(a, b). The real part of the dielectric constant is correlated to the dispersion, which is linked with the speed of light through the materials, while the complex dielectric constant is considered an intrinsic material property that indicates a dissipative rate [62]. Both the real and imaginary parts of the dielectric constant show dominance in the ultra-violet region, and its dominancy decreases with increasing doping concentration.

Finally, the optical conductivity (σ_{op}) is measured using Eq. (11),

$$\sigma_{op} = \alpha nc \tag{11}$$

where α is the absorption coefficient, n is the refractive index, and c is the speed of light. The variance of optical conductivity with wavelength for pure and Fe-doped CuO thin films is presented in Figure 6(c). Pure CuO thin films have the highest optical conductivity in the UV region, which is attributed to their high absorbance, and with increasing doping concentration, the values decrease drastically.

3.4. Antimicrobial properties

The inhibitory antibacterial potential exhibited by undoped and Fe-doped CuO thin films against both gram-positive and gram-negative bacterial strains was studied [63]. The antibacterial activities of synthesized CuO thin films with Fe doping displayed reliable bactericidal activity that may be useful in biomedical applications [64]. The antibacterial analysis of these thin films against both gram-positive and gram-negative bacteria using the agar well diffusion technique revealed the toxicity of CuO in killing the growth of the examined pathogens. The performances are presented in Figure 7 and summarized in Table 3.

Pristine CuO showed good antimicrobial activity in all media, and the highest ZOI of 12 mm was observed for aureus. The antibacterial properties of 3 wt.% Fe doped CuO decreased slightly from pristine, whereas the antifungal activity increased slightly. Antifungal activity increased continuously with increasing dopant amount and the highest ZOI of 13 mm was observed for 9 wt.% Fe doped CuO. Similar improvements were reported for Fe-doped CuO nanoparticles due to easy binding and penetration in the cell [65]. The antibacterial properties of 6 wt.% Fe and 9 wt.% Fe doped CuO were similar, except for *B. cereus*, where 6 wt.% Fe doped CuO showed greater ZOI. V-doped CuO thin films synthesized by dip-coating show parallel outputs in the range of 10–15 mm ZOI for E. coli and S. aureus [44]. Similarly, Zn-doped CuO nanostructures have ZOI of 7–16 mm for S. aureus and E. coli [66].

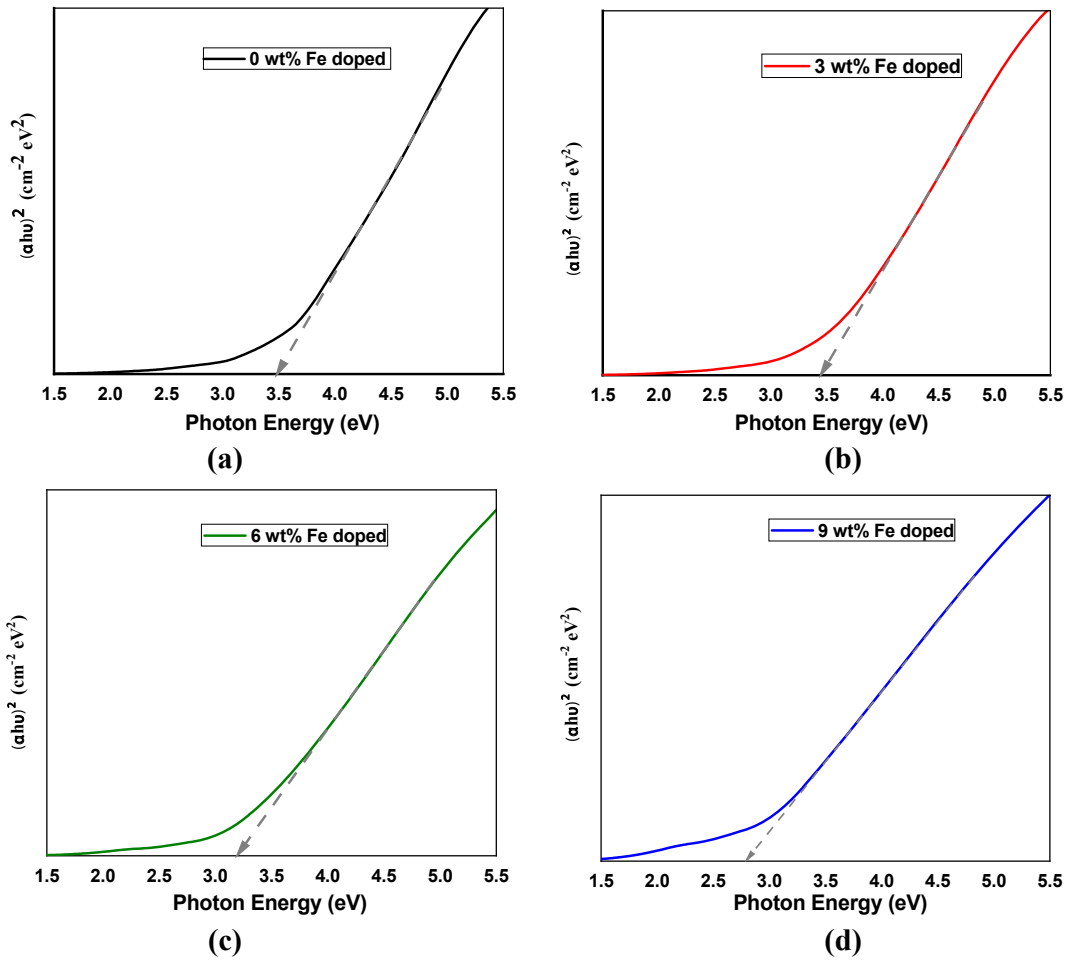

Figure 4. Tauc's plots for calculating optical direct band gap of (a) pure CuO, (b) 3 wt.% (c) 6 wt.%, and (d) 9 wt.% Fe-doped CuO thin films.

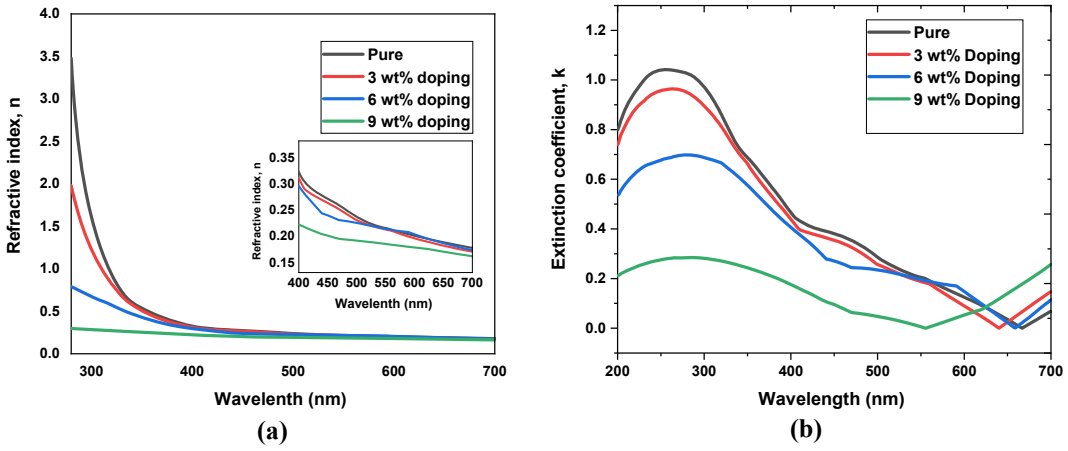

Figure 5. (a) Refractive index and (b) extinction coefficient of pure and Fe-doped CuO thin films.

Reactive oxygen species (OH, H_2O_2, and O_2^-) generated by CuO may interact with the bacterial cell membrane to facilitate the penetration of CuO into the bacterial cell [67]. Interference of CuO with the bacterial cell membrane results in several malfunctions that prevent the growth of the bacterial species and may ultimately cause their death [68]. The smaller size of CuO (nanometer) compared to the pore size of bacterial cells (micrometer) allows the easy penetration of CuO into the cell membrane [69]. The destruction of the bacterial membranes by CuO could be via the production of reactive oxygen species and radicals or by direct cell damage since superoxide, and hydroxyl radicals are produced by metal oxides (CuO) [70]. Moreover, Cu^{2+} ions may be drawn to the bacterial cell surface due to the prevalence of carboxyl and amine groups [68, 69, 70]. Therefore, the probable antibacterial mechanism can be associated with gene toxicity, mechanical damage, or oxidative injury.

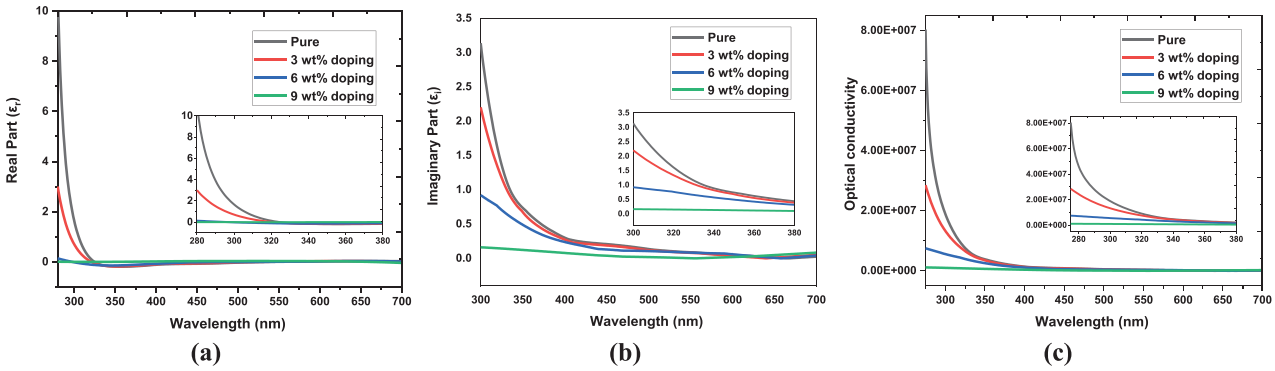

Figure 6. (a) Real and (b) imaginary part of dielectric constant and (c) optical conductivity of pure and Fe-doped CuO thin films.

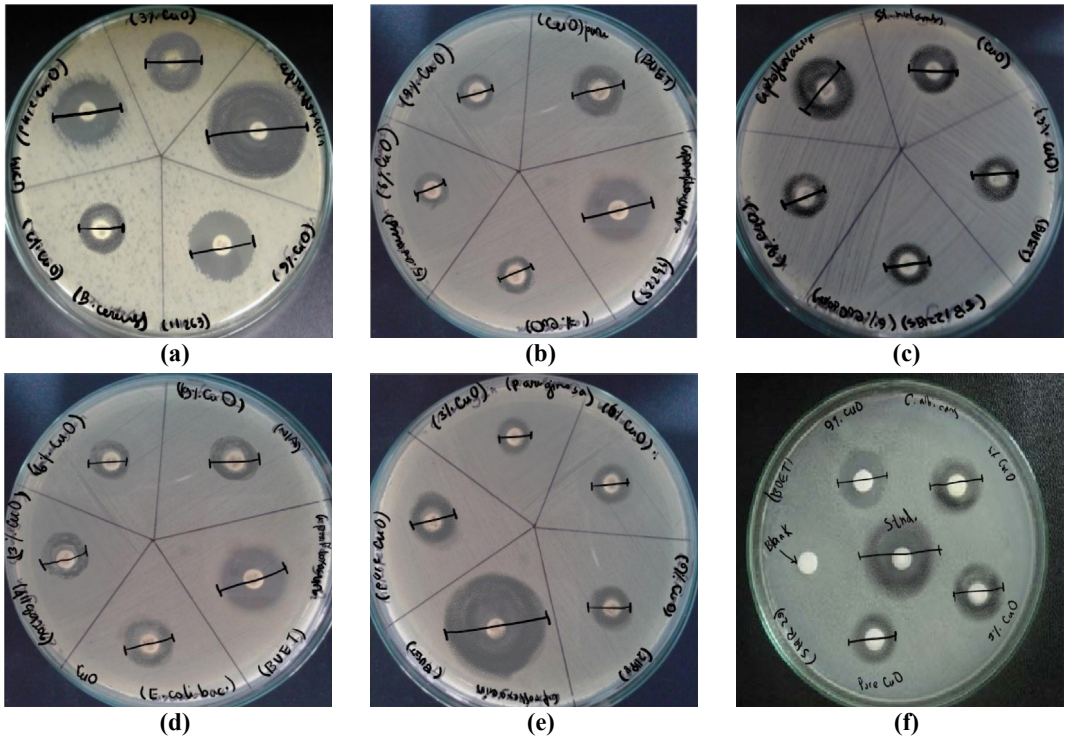

Figure 7. Zone of Incubation (ZOI) created by CuO and Fe-doped CuO against (a) *Bacillus cereus*, (b) *Staphylococcus aureus*, (c) Streptococcus mutans, (d) *Escherichia coli*, (e) *Pseudomonas aruginosa*, and (f) *Candida albicans*.

Table 3. Antimicrobial activity of pure and Fe-doped CuO thin films.

Type	Gram-Positive			Gram-Negative		Fungus
Bacteria	Bacillus cereus	Staphylococcus aureus	Streptococcus mutans	Escherichia coli	Pseudomonas aruginosa	Candida albicans
Dopant Concentration	Zone of Inhibition (mm)					
0 wt.%	10	12	10	11	9	9
3 wt.%	8	7	8	10	8	10
6 wt.%	7	8	8	11	6	12
9 wt.%	9	8	8	11	6	13
Standard Ciprofloxaine	18	19	18	18	19	18
						Standard Clotrimazole

4. Conclusions

Pure CuO and Fe-doped CuO thin films were synthesized by sol-gel spin coating technique and the structural, optical, and antimicrobial properties of these films were studied. XRD spectra revealed that all the samples were polycrystalline with preferential ($\bar{1}11$) and (111) orientations. The crystallite size, dislocation density, strain, lattice parameter, and cell volume were calculated by Rietveld refinement. Our investiga-

tion showed that Fe-doping has a significant impact on CuO thin films. Increasing grain size with uniform size distribution can be achieved from Fe doping. Moreover, the bandgap of pure CuO thin film can be controlled in the range of 3.48 to 2.79 eV due to band tailing effects. Several optical properties were estimated, and it was determined that these parameters are highly modifiable via Fe-doping. In the antimicrobial study, it was discovered that Fe-doped thin films were efficacious against Escherichia coli and Candida albicans, among other bacteria and fungi. In conclusion, the prepared nanostructured thin films for Fe-doped CuO can be recommended for optoelectronic and biomedical industries.

Declarations

Author contribution statement

Mohammad Humaun Kabir, Humayra Ibrahim: Performed the experiments; Analyzed and interpreted the data; Wrote the paper. Sikder Ashikuzzaman Ayon: Analyzed and interpreted the data; Wrote the paper. Md Muktadir Billah: Conceived and designed the experiments; Analyzed and interpreted the data; Contributed reagents, materials, analysis tools or data; Wrote the paper. Sharif Neaz: Performed the experiments.

Funding statement

This work was supported by the Department of Materials and Metallurgical Engineering (MME), Bangladesh University of Engineering and Technology (BUET).

Data availability statement

No data was used for the research described in the article.

Declaration of interests statement

The authors declare no conflict of interest.

Additional information

No additional information is available for this paper.

References

[1] S. Dolai, R. Dey, S. Das, S. Hussain, R. Bhar, A.K. Pal, Cupric oxide (CuO) thin films prepared by reactive d.c. Magnetron sputtering technique for photovoltaic application, J. Alloys Compd. 724 (2017) 456.
[2] P. Kumar, M. Chandra Mathpal, J. Prakash, B.C. Viljoen, W.D. Roos, H.C. Swart, Band gap tailoring of cauliflower-shaped CuO nanostructures by Zn doping for antibacterial applications, J. Alloys Compd. 832 (2020).
[3] L. Liao, et al., Multifunctional CuO nanowire devices: P-type field effect transistors and CO gas sensors, Nanotechnology 20 (2009).
[4] Y.J. Park, J.H. Yang, B.D. Ryu, J. Cho, T.V. Cuong, C.-H. Hong, Solution-processed multidimensional ZnO/CuO heterojunction as ultraviolet sensing, Opt. Mater. Express 5 (2015) 1752.
[5] M.M. Rashad, D.A. Rayan, A.A. Ramadan, Optical and magnetic properties of CuO/CuFe2O4 nanocomposites, J. Mater. Sci. Mater. Electron. 24 (2013) 2742.
[6] S. Ebrahim Moosavifard, M.F. El-Kady, M.S. Rahmanifar, R.B. Kaner, M. Fazlollah Mousavi, S.E. Moosavifard, M.F. Mousavi, Designing 3D Highly Ordered Nanoporous CuO Electrodes for High-Performance Asymmetric Supercapacitors, 2015.
[7] X. Zhao, P. Wang, Z. Yan, N. Ren, Room temperature photoluminescence properties of CuO nanowire arrays, Opt. Mater. 42 (2015).
[8] S.G. Ovchinnikov, B.A. Gizhevskiĭ, Y.P. Sukhorukov, A.E. Ermakov, M.A. Uĭmin, E.A. Kozlov, Y.A. Kotov, A.v. Bagazeev, Specific features of the electronic structure and optical spectra of nanoparticles with strong electron correlations, Phys. Solid State 49 (2007) 1116.
[9] Y. Kwon, J. Gyeong, M. Choi$, Nonstoichiometry at TD Electrical Conduction of 010, 1996.
[10] T. Koh, E. O'Hara, M.J. Gordon, Growth of nanostructured CuO thin films via microplasma-assisted, reactive chemical vapor deposition at high pressures, J. Cryst. Growth 363 (2013) 69.
[11] M. Petrantoni, C. Rossi, L. Salvagnac, V. Conédéra, A. Estève, C. Tenailleau, P. Alphonse, Y.J. Chabal, Multilayered Al/CuO thermite formation by reactive magnetron sputtering: nano versus micro, J. Appl. Phys. 108 (2010).
[12] R.P. Wijesundera, Fabrication of the CuO/Cu2O heterojunction using an electrodeposition technique for solar cell applications, Semicond. Sci. Technol. 25 (2010).
[13] K. Mageshwari, D. Nataraj, T. Pal, R. Sathyamoorthy, J. Park, Improved photocatalytic activity of ZnO coupled CuO nanocomposites synthesized by reflux condensation method, J. Alloys Compd. 625 (2015) 362.
[14] K. Mageshwari, R. Sathyamoorthy, Physical properties of nanocrystalline CuO thin films prepared by the SILAR method, Mater. Sci. Semicond. Process. 16 (2013) 337.
[15] M.H. Kabir, H. Ibrahim, M.M. Billah, Effect of stabilizer on sol ageing for CuO thin films synthesized by sol-gel spin coating technique, in: AIP Conference Proceedings 2324, American Institute of Physics Inc., 2021.
[16] B. Allabergenov, U. Shaislamov, H. Shim, M.-J. Lee, A. Matnazarov, B. Choi, Effective control over near band-edge emission in ZnO/CuO multilayered films, Opt. Mater. Express 7 (2017) 494.
[17] G. Shetty, V. Crasta, R. Kumar, R.K.R. Bairy, P. Shankaragouda Patil, Promising PVA/TiO2, CuO filled nanocomposites for electrical and third order nonlinear optical applications, Opt. Mater. 95 (2019).
[18] Y.F. Lim, C.S. Chua, C.J.J. Lee, D. Chi, Sol-gel deposited Cu2O and CuO thin films for photocatalytic water splitting, Phys. Chem. Chem. Phys. 16 (2014), 25928.
[19] R.R. Prabhu, A.C. Saritha, M.R. Shijeesh, M.K. Jayaraj, Fabrication of P-CuO/n-ZnO heterojunction diode via sol-gel spin coating technique, Mater. Sci. Eng. B 220 (2017) 82.
[20] S. Baturay, A. Tombak, D. Kaya, Y.S. Ocak, M. Tokus, M. Aydemir, T. Kilicoglu, Modification of electrical and optical properties of CuO thin films by Ni doping, J. Sol. Gel Sci. Technol. 78 (2016) 422.
[21] M. Heinemann, B. Eifert, C. Heiliger, Band structure and phase stability of the copper oxides Cu2O, CuO, and Cu4O3, Phys. Rev. B Condens. Matter 87 (2013).
[22] J. Wu, K.S. Hui, K.N. Hui, L. Li, H.H. Chun, Y.R. Cho, Characterization of Sn-doped CuO thin films prepared by a sol–gel method, J. Mater. Sci. Mater. Electron. 27 (2016) 1719.
[23] J. Uddin, M. Sharmin, M.N. Hasan, J. Podder, Influence of Ni doping on the morphological, structural, optical and electrical properties of CuO thin films deposited via a spray pyrolysis, Opt. Mater. 119 (2021).
[24] A. Rydosz, A. Szkudlarek, Gas-sensing performance of M-doped CuO-based thin films working at different temperatures upon exposure to propane, Sensors 15 (2015).
[25] A. Yildiz, Horzum, N. Serin, T. Serin, Hopping conduction in in-doped CuO thin films, in: Applied Surface Science 318, 2014.
[26] F. Bayansal, T. Taşköprü, B. Şahin, H.A. Çetinkara, Effect of cobalt doping on nanostructured CuO thin films, Metall. Mater. Trans. A 45 (2014).
[27] M.R. Das, P. Mitra, Influence of nickel incorporation on structural, optical and electrical characteristics of SILAR synthesized CuO thin films, J. Sol. Gel Sci. Technol. 87 (2018).
[28] J. Oh, H. Ryu, W.J. Lee, J.S. Bae, Improved photostability of a CuO photoelectrode with Ni-doped seed layer, Ceram. Int. 44 (2018).
[29] S. Ruzgar, Y. Caglar, O. Polat, D. Sobola, M. Caglar, Tuning the optical properties of Fe-doped CuxO thin films synthesized via the sol–gel spin-coating method, Appl. Phys. Mater. Sci. Process 127 (2021).
[30] Y. Wang, T. Jiang, D. Meng, D. Wang, M. Yu, Synthesis and enhanced photocatalytic property of feather-like Cd-doped CuO nanostructures by hydrothermal method, Appl. Surf. Sci. 355 (2015).
[31] T. Gnanasekar, S. Valanarasu, I.L. Poul Raj, A.V. Juliet, P.K. Behera, Z.M.M. Mahmoud, M. Shkir, S. AlFaify, Improved photocurrent properties of La doped CuO thin films coated by nebulizer spray pyrolysis method for photosensor applications, Opt. Mater. 122 (2021).
[32] A.M. Ahmed, E.M. Abdalla, M. Shaban, Simple and low-cost synthesis of Ba-doped CuO thin films for highly efficient solar generation of hydrogen, J. Phys. Chem. C 124 (2020).
[33] A.A. Menazea, A.M. Mostafa, Ag doped CuO thin film prepared via pulsed laser deposition for 4-nitrophenol degradation, J. Environ. Chem. Eng. 8 (2020).
[34] A.M. el Sayed, M. Shaban, Structural, optical and photocatalytic properties of Fe and (Co, Fe) Co-doped copper oxide spin coated films, Spectrochim. Acta, Part A 149 (2015) 638.
[35] J.S. Shaikh, R.C. Pawar, R.S. Devan, Y.R. Ma, P.P. Salvi, S.S. Kolekar, P.S. Patil, Synthesis and characterization of Ru doped CuO thin films for supercapacitor based on bronsted acidic ionic liquid, Electrochim. Acta 56 (2011).
[36] J. Zhao, Q. Xia, J. Li, Ferromagnetism in Fe-doped CuO nanopowder, J. Semiconduct. 33 (2012).
[37] F. Zhao, H.M. Qiu, L.Q. Pan, H. Zhu, Y.P. Zhang, Z.G. Guo, J.H. Yin, X.D. Zhao, J.Q. Xiao, Ferromagnetism analysis of Mn-doped CuO thin films, J. Phys. Condens. Matter 20 (2008).
[38] S. Manna, S.K. De, Room temperature ferromagnetism in Fe doped CuO nanorods, J. Magn. Magn Mater. 322 (2010).
[39] D. Paul Joseph, C. Venkateswaran, S. Sambasivam, B.C. Choi, Effect of Fe alloying on the structural, optical, electrical and magnetic properties of spray-deposited CuO thin films, J. Kor. Phys. Soc. 61 (2012).
[40] N.R. Panda, B.S. Acharya, P. Nayak, S.P. Pati, B.K. Nath, D. Das, Role of Cr 3 ions on superexchange coupling in α-Fe 2O 3 nanoparticles, Phys. B Condens. Matter 407 (2012).
[41] H. Zhu, F. Zhao, L. Pan, Y. Zhang, C. Fan, Y. Zhang, J.Q. Xiao, Structural and magnetic properties of Mn-doped CuO thin films, J. Appl. Phys. 101 (2007).
[42] S.G. Yang, T. Li, B.X. Gu, Y.W. Du, H.Y. Sung, S.T. Hung, C.Y. Wong, A.B. Pakhomov, Ferromagnetism in Mn-doped CuO, Appl. Phys. Lett. 83 (2003).

[43] M.M. Momeni, M. Mirhosseini, Z. Nazari, A. Kazempour, M. Hakimiyan, Antibacterial and photocatalytic activity of CuO nanostructure films with different morphology, J. Mater. Sci. Mater. Electron. 27 (2016).
[44] Z.N. Kayani, H. Aslam, Investigation of structural, optical, antibacterial, and dielectric properties of V-doped copper oxide thin films: comparison with undoped copper oxide thin films, Adv. Powder Technol. 32 (2021).
[45] J. Oh, H. Ryu, W.J. Lee, Effects of Fe doping on the photoelectrochemical properties of CuO photoelectrodes, Compos. B Eng. 163 (2019).
[46] F.Z. Chafi, L. Bahmad, N. Hassanain, B. Fares, L. Laanab, A. Mzerd, Characterization Techniques of Fe-Doped Cuo Thin Films Deposited by the Spray Pyrolysis Method, 2018 arXiv.
[47] C. Valgas, S. Machado De Souza, F. A. Smânia, A. Smânia, Screening methods to determine antibacterial activity of natural products, Braz. J. Microbiol. 38 (2007) 369.
[48] S.A. Shehata, S.A. Bader, Effect of nile river water quality on algal distribution at Cairo, Egypt, Environ. Int. (1985).
[49] M. Dhaouadi, Physical properties of copper oxide thin films prepared by sol–gel spin–coating method, Am. J. Phys. Appl. 6 (2018) 43.
[50] S. Layek, H.C. Verma, Room temperature ferromagnetism in Fe-doped CuO nanoparticles, J. Nanosci. Nanotechnol. 13 (2013) 1848.
[51] M.M. Hassan, W. Khan, A. Azam, A.H. Naqvi, Effect of size reduction on structural and optical properties of ZnO matrix due to successive doping of Fe ions, J. Lumin. 145 (2014) 160.
[52] Y. Li, M. Xu, L. Pan, Y. Zhang, Z. Guo, C. Bi, Structural and room-temperature ferromagnetic properties of Fe-doped CuO nanocrystals, J. Appl. Phys. 107 (2010).
[53] P. Chand, A. Gaur, A. Kumar, U. Kumar Gaur, Structural and optical study of Li doped CuO thin films on Si (1 0 0) substrate deposited by pulsed laser deposition, Appl. Surf. Sci. 307 (2014) 280.
[54] Ş. Baturay, A. Tombak, D. Batibay, Y.S. Ocak, N-type conductivity of CuO thin films by metal doping, Appl. Surf. Sci. 477 (2019) 91.
[55] T. Chtouki, S. Taboukhat, H. Kavak, A. Zawadzka, H. Erguig, B. Elidrissi, B. Sahraoui, Characterization and third harmonic generation calculations of undoped and doped spin-coated multilayered CuO thin films, J. Phys. Chem. Solid. 124 (2019) 60.
[56] E.G. Goh, X. Xu, P.G. McCormick, Effect of particle size on the UV absorbance of zinc oxide nanoparticles, Scripta Mater. 78–79 (2014) 49.
[57] N.M. Basith, J.J. Vijaya, L.J. Kennedy, M. Bououdina, Structural, morphological, optical, and magnetic properties of Ni-doped CuO nanostructures prepared by a rapid microwave combustion method, Mater. Sci. Semicond. Process. 17 (2014) 110.
[58] M. Umadevi, A. Jegatha Christy, Synthesis, characterization and photocatalytic activity of CuO nanoflowers, Spectrochim. Acta, Part A 109 (2013) 133.
[59] P. van Mieghem, Theory of Band Tails in Heavily Doped Semiconductors A Particle in a One-Dimensional Random Potential, 1992.
[60] T. Shrividhya, G. Ravi, Y. Hayakawa, T. Mahalingam, Determination of structural and optical parameters of CuO thin films prepared by double dip technique, J. Mater. Sci. Mater. Electron. 25 (2014) 3885.
[61] A. Moumen, B. Hartiti, E. Comini, Z. el khalidi, H.M.M.M. Arachchige, S. Fadili, P. Thevenin, Preparation and characterization of nanostructured CuO thin films using spray pyrolysis technique, Superlattice. Microst. 127 (2019) 2.
[62] V. Ramya, K. Neyvasagam, R. Chandramohan, S. Valanarasu, A.M.F. Benial, Studies on chemical bath deposited CuO thin films for solar cells application, J. Mater. Sci. Mater. Electron. 26 (2015) 8489.
[63] A. Azam, A.S. Ahmed, M. Oves, M.S. Khan, A. Memic, Size-dependent antimicrobial properties of CuO nanoparticles against gram-positive and -negative bacterial strains, Int. J. Nanomed. 7 (2012) 3527.
[64] G. Sharmila, M. Thirumarimurugan, V.M. Sivakumar, Optical, catalytic and antibacterial properties of phytofabricated CuO nanoparticles using tecoma castanifolia leaf extract, Optik 127 (2016) 7822.
[65] A. Pugazhendhi, S.S. Kumar, M. Manikandan, M. Saravanan, Photocatalytic properties and antimicrobial efficacy of Fe doped CuO nanoparticles against the pathogenic bacteria and fungi, Microb. Pathog. 122 (2018).
[66] A. Khalid, et al., Structural, optical and antibacterial efficacy of pure and zinc-doped copper oxide against pathogenic bacteria, Nanomaterials 11 (2021).
[67] S.A. Ayon, M.M. Billah, S.S. Nishat, A. Kabir, Enhanced photocatalytic activity of Ho3+ doped ZnO NPs synthesized by modified sol-gel method: an experimental and theoretical investigation, J. Alloys Compd. 856 (2021).
[68] D. Das, B.C. Nath, P. Phukon, S.K. Dolui, Synthesis and evaluation of antioxidant and antibacterial behavior of CuO nanoparticles, Colloids Surf. B Biointerfaces 101 (2013) 430.
[69] P. Sutradhar, M. Saha, D. Maiti, Microwave synthesis of copper oxide nanoparticles using tea leaf and coffee powder extracts and its antibacterial activity, J. Nanostruc. Chem. 4 (2014).
[70] Y.N. Chang, M. Zhang, L. Xia, J. Zhang, G. Xing, The toxic effects and mechanisms of CuO and ZnO nanoparticles, Materials (2012).